jugated acids correspond to O_4-H, N_3-H, N_1-H, and N_7-H protonated species, respectively. The same protonation sites were experimentally determined for the corresponding deoxynucleosides in solution[29] and in the solid state.[30] If the examined clusters are formed under equilibrium conditions, by recombination in the selvedge,[3] it can be assumed that the same sites are involved in the formation of the proton-bound dimers. Nevertheless, the population of different tautomers does not alter the main observation related to the basicity order of the examined species.

The enhanced basicity of the deoxynucleosides over the corresponding bases was explained to be due to the formation of intramolecular hydrogen bonds among the base and the sugar moieties.[14] An alternative explanation for the observed phenomenon can consider the electron-donating effect exerted by the deoxyribose on the linked purine or pyrimidine rings. The inversion of the basicity order of dA and dC, which indeed exhibit very similar PA's, with respect to their corresponding nucleobases Ade and Cyt, might be due to different effects exerted by the deoxyribose unit. This borderline situation accounts for the observed slight preference in the formation of $[dA+H]^+$ in the dissociation of $[dA+dC+H]^+$ species.[11] In the latter case, however, it must be considered that mixtures of multiple hydrogen-bonded pairs can be formed,[13] which affect the unimolecular dissociation of the cluster, and thus, an accurate estimation of the relative proton affinities of the two interacting components.

Conclusion

Fast atom bombardment methodology can be used to form protonated heterocomplexes, whose gas-phase unimolecular dissociations can provide a probe of their relative proton affinities. This kinetic approach has given, for the first time, stratightforward information on the relative basicity scale of DNA nucleosides and related nucleobases in the absence of solvent effect. The experimental PA order dG > dA = dC ≫ dT differs from that of the corresponding nucleobases, Gua > Cyt > Ade ≫ Thy, evaluated under the same conditions. The uniqueness of the applied methodology lies in the fact that a clear distinction has been made among the gas-phase basicity of the most basic nucleosides and corresponding nucleobases, which possess very similar proton affinity properties.

Experimental Section

Deoxynucleosides, pyrimidines, and purines were purchased from Fluka; amines and matrices were purchased from Aldrich. Saturated solutions (1-2 μL) of nucleic acid materials and the appropriate amines were deposited on the target of the FAB probe. When H_2O was used as the matrix, the corresponding solutions were frozen by dipping the covered target into liquid nitrogen. Mass spectra were obtained on a Vacuum Generators (VG) ZAB-2F instrument operated at an accelerating potential of 8 kV by using the M-SCAN steerable FAB gun. A neutral Xe beam of 9.5 keV energy and a neutral current of ca. 10 μA were employed. The spectra were recorded at 1000 resolution by scanning the magnetic field. The MIKE spectra were recorded by scanning down the electrostatic sector potential. The standard deviations on the k_N/k_a values were determined from five independent measurements, and the error propagation on the calculated PA's was computed from the squared partial derivative of eq 7.

Acknowledgment. This work was supported by the Ministero della Pubblica Istruzione (M.P.I. 40% grant) and by the "Progetto Finalizzato Chimica Fine II del CNR".

Registry No. dA, 958-09-8; dC, 951-77-9; dG, 961-07-9; dT, 50-89-5; Ade, 73-24-5; Cyt, 71-30-7; Gua, 73-40-5; Thy, 65-71-4.

(28) Del Bene, J. E. *J. Phys. Chem.* **1983**, *87*, 367.
(29) Izatt, R. M.; Christensen, J. J.; Rytting, J. H. *Chem. Rev.* **1971**, *71*, 439-481.
(30) Taylor, R.; Kennard, O. *J. Mol. Struct.* **1982**, *78*, 1-28.

Metal-Assisted Hydroformylation on a SiO_2-Attached Rh Dimer. In Situ EXAFS and FT-IR Observations of the Dynamic Behaviors of the Dimer Site

Kiyotaka Asakura,[†] Kyoko Kitamura-Bando,[†] Yasuhiro Iwasawa,*[,†] Hironori Arakawa,[‡] and Kiyoshi Isobe[§]

Contribution from the Department of Chemistry, Faculty of Science, University of Tokyo, Hongo, Bunkyo-ku, Tokyo 113, Japan, National Chemical Laboratory for Industry, Higashi, Tsukuba, Ibaraki 305, Japan, and Institute for Molecular Science, 38, Nishigonaka, Myodaiji, Okazaki, Aichi 444, Japan. *Received March 12, 1990*

Abstract: *trans*-$[Rh(C_5Me_5)(CH_3)]_2(\mu\text{-}CH_2)_2$ was supported on the SiO_2 surface by the reaction with OH groups of SiO_2 at 313 K, followed by evacuation at 373 K. In this attaching reaction, the Rh dimer complexes were bound to the SiO_2 surface through Rh-O(surface) bonds, losing one CH_3 ligand and one C_5Me_5 ligand per Rh dimer. The attached Rh dimers were found to be more active and selective than a conventionally prepared Rh/SiO_2 catalyst. The structure change of the Rh dimer sites in each reaction step for catalytic hydroformylation was followed by means of in situ FT-IR and in situ EXAFS techniques. The Rh-Rh bond in the attached Rh dimers (Rh-Rh = 0.262 nm) was cleaved by CO adsorption to form monomer pairs $[Rh(C_2H_5)(CO)_2(O\text{-}Si) + Rh(C_5Me_5)(O\text{-}Si)]$. Heating the monomer pairs to 423 K under vacuum resulted in CO insertion, with new peaks exhibited at 1710 and 1394 cm^{-1} due to the acyl ligand. The insertion was promoted by rebonding of the two adjacent Rh atoms observed at 0.270 nm. The Rh-acyl dimers were reversibly converted to the previous monomer pairs without Rh-Rh bonding by CO admission. These behaviors of Rh dimers on SiO_2 are entirely different from usual Rh monomer chemistry. A new metal-assisted reaction mechanism is described.

Introduction

Organometallic dimers and clusters have been widely studied in order to prepare dispersed metal sites with well-defined compositions on inorganic supports and to elucidate catalytic reaction mechanisms on a molecular level.[1-3] Irrespective of definite structures and compositions of starting metal clusters, the relationship between structure and catalytic performance is often poorly defined and catalytic sites remain unidentified because we

[†] University of Tokyo.
[‡] National Chemical Laboratory for Industry.
[§] Institute for Molecular Science.

(1) Gates, B. C., Guczi, L., Knözinger, H., Eds. *Metal Clusters in Catalysis. Studies in Surface Science and Catalysis 29*; Elsevier: New York, 1986.
(2) Yermakov, Y. I.; Kuznetsov, B. N.; Zakharov, V. *Catalysis by Supported Complexes*; Elsevier: Amsterdam, 1981.
(3) Iwasawa, Y., Ed.: *Tailored Metal Catalysts*; D. Reidel: Holland, 1986.

0002-7863/90/1512-9096$02.50/0

have only limited techniques to obtain direct structural information on catalyst surfaces. Furthermore, the structures of the supported metal sites have been demonstrated to change dynamically under the catalytic conditions.[4-7] Therefore, in situ spectroscopic experiments with catalysts under the working conditions are required for the full understanding of solid catalysis. EXAFS spectroscopy has made it possible for the first time to determine the local structure around the metal atom in supported metal catalysts.[8-10] It allowed us to investigate the structural change of the Mo dimer catalyst in the course of oxidation of C_2H_5OH.[11]

In this paper, we report the catalytic performance and dynamic behavior of a Rh dimer catalyst derived from *trans*-$[Rh(C_5Me_5)(CH_3)]_2(\mu\text{-}CH_2)_2$ in ethene hydroformylation reactions by means of both in situ FT-IR and in situ EXAFS spectroscopies. SiO_2-supported Rh catalysts are known as good catalysts for CO hydrogenation to selectively produce C_2-oxygenated compounds,[12] while Rh monomer complexes have been used as hydroformylation catalysts in homogeneous systems.[13] The CO-insertion (alkyl migration) reaction is an important key step in these reactions. The reaction mechanism for CO insertion has been discussed on the basis of mononuclear organometallic chemistry,[14,15] while the role of the metal–metal bond in supported-metal catalysis has been little recognized.[16-18] In order to explore the role of metal–metal bonding in the CO-insertion reaction and its related catalytic reaction, we chose the Rh dimer complex $[Rh(C_5Me_5)(CH_3)]_2(\mu\text{-}CH_2)_2$, which has a CH_3 ligand and a C_5Me_5 ligand on the Rh atom. If a C_5Me_5 ligand in the dimer was lost and another C_5Me_5 ligand remained on a Rh atom, the C_5Me_5-free Rh atom would act as a reaction site and the adjacent Rh atom with a large C_5Me_5 ligand would hardly be accessible to reactant molecules. Thus, it is possible to examine the catalytic activity of the C_5Me_5-free Rh atom and the role of the adjacent Rh atom. We have prepared such Rh dimers on the SiO_2 surface by the reaction of $[Rh(C_5Me_5)(CH_3)]_2(\mu\text{-}CH_2)_2$ with surface OH groups of SiO_2. The Rh dimer complex also has CH_3 and CH_2 ligands, which may be species active for CO insertion.

In this paper, we characterize the attached structure of the Rh dimer. The interesting features of attached Rh dimers in the interaction of CO are described, and the cause for this interesting phenomenon is given on the basis of the molecular structure of the Rh dimer. The purpose of this work is to develop a new Rh dimer catalyst for the hydroformylation reaction and to reveal the importance of Rh–Rh metal bonding in the CO-insertion reaction. We propose a metal-assisted CO-insertion mechanism on the basis of in situ spectroscopic characterizations of the Rh structures.

Experimental Section

The incipient SiO_2-attached Rh dimer was prepared by the reaction of *trans*-$[Rh(C_5Me_5)(CH_3)]_2(\mu\text{-}CH_2)_2$ with surface OH groups of SiO_2 in the pentane or deuterated benzene solution. The complex was synthesized in a way similar to that previously reported.[19] Pentane was purified by reflux over Na wire, followed by distillation. Commercially available deuterated benzene (Aldrich 99.5 atom % D) was used without further purification. SiO_2 (Aerosil 300; surface area, 300 m^2/g) was evacuated at 673 K for 1 h before use as support to control the surface OH concentration at 2 OH nm^{-2}. The Rh loading on SiO_2 was 1 wt % as Rh/support. All the procedures were carried out under vacuum or high-purity (99.9995%) Ar atmosphere because the attached sample was sensitive to air, unlike the original Rh dimer complex. The deuterated-methyl Rh dimer complexes $[Rh(C_5Me_5\text{-}d)(CH_3)]_2(\mu\text{-}CH_2)_2$ and $[Rh(C_5Me_5\text{-}d)(CD_3)]_2(\mu\text{-}CH_2)_2$[20] were also synthesized to prepare the SiO_2-attached deuterated Rh dimers in order to separate the ν(C–H) bands of $\mu\text{-}CH_2$ and CH_3 ligands from the complicated methyl bands of C_5Me_5. The sample was then treated under vacuum at 313 K for 0.5 h and at 373 K for 0.5 h to complete the surface reaction between the Rh dimer and the surface OH groups. We denoted the Rh dimers at this stage as species A.

Table I. Curve-Fitting Analysis for EXAFS Data of Reference Rh Complexes by Use of Theoretical Parameters[24,25]

sample	bonding	CN	distance/nm	
			EXAFS	X-ray
Rh metal	Rh–Rh	12	0.266 ± 0.002	0.268
Rh_2O_3	Rh–O	6	0.203 ± 0.003	0.205
$Rh_2(CO)_4Cl_2$	Rh–C	2	0.183 ± 0.002	0.181
	Rh–Cl	2	0.233 ± 0.003	0.2355
	Rh---O	2	0.298 ± 0.002	0.298
$Rh_6(CO)_{16}$	Rh–C(terminal)	2.1 ± 0.5	0.193 ± 0.003	0.186
	Rh–C(bridge)	2.2 ± 0.5	0.227 ± 0.003	0.217
	Rh–Rh	4.0 ± 0.5	0.276 ± 0.003	0.278
	Rh---O	4.1 ± 0.2	0.299 ± 0.002	0.298

The surface species A and its surface behaviors were characterized by IR and EXAFS spectroscopies under in situ conditions. Rh K-edge EXAFS spectra were taken in a transmission mode at BL 10B of Photon Factory in the National Laboratory for High-Energy Physics (KEK-PF) with a Si(311) channel-cut monochromator.[21] The estimated energy resolution is 7 eV.[21] The spectra were recorded at room temperature. The 17- and 34-cm ionization chambers were used as detectors for I_0 and I signals filled with Ar gas. The second harmonic is eliminated, owing to the extinction rule of the Si(311), and the third and higher harmonics could be neglected, owing to the low efficiency of the Ar gas in the ionization chamber and the low intensity of the photons with corresponding energy emitted from the storage ring. To obtain the in situ EXAFS spectra, we used a glass EXAFS cell with two thin-glass windows in which no Rh impurity was detected. The in situ EXAFS cell was connected to a closed circulating system through a stopcock. We used EXAFS formula 1 in the curve-fitting analysis of EXAFS data,[22,23]

$$\chi(k'_j) = \sum S_j N_j F_j(k'_j) \exp(-2k'^2_j\sigma_j^2) \sin(2k'_j r_j + \phi_j(k'_j))/k'_j r_j^2 \quad (1)$$

$$k'_j = (k^2 - 2m\Delta E_j/\hbar^2)^{1/2}$$

where k_j is the photoelectron wavenumber, $F_j(k')$ is the backscattering amplitude function, and $\phi_j(k')$ is the phase shift function. Both theoretical and empirical phase shift ($\phi_j(k')$) and amplitude functions ($F_j(k')$) were used. Model compounds used were Rh metal, Rh_2O_3, and $[Rh(CO)_2]_2Cl_2$ for Rh–Rh, Rh–O, and Rh---O(carbonyl), respectively. The theoretical parameters used here have been given by Teo and Lee.[24] We also used theoretically derived phase shift and amplitude functions, including multiple scattering for Rh---O.[25] Validity for the theoretically derived parameters was checked as shown in Table I. S_j is the amplitude reduction factor that arises from many-body effects and inelastic losses in the scattering process. This value can be regarded as a constant function of k because both factors have opposite k dependence.[22] S_j is determined by fitting the model compounds by use of the theoretical

(4) Van't Blik, H. F. J.; Van Zon, J. B. A. D.; Huizinger, T.; Vis, J. C.; Koningsberger, D. C.; Prins, R. *J. Phys. Chem.* **1983**, *87*, 2264.
(5) Iwasawa, Y. *Adv. Catal.* **1987**, *35*, 187.
(6) Iwasawa, Y.; Gates, B. C. *CHEMTECH* **1989**, 173.
(7) Asakura, K.; Iwasawa, Y. *J. Phys. Chem.* **1989**, *93*, 4213.
(8) Lytle, F. W.; Via, G. H.; Sinfelt, J. H. *J. Chem. Phys.* **1977**, *67*, 3831.
(9) Sinfelt, J. H.; Via, G. H.; Lytle, F. W. *Catal. Rev. Sci. Eng.* **1984**, *26*, 81.
(10) Bart, J. C. J.; Vlaic, G. *Adv. Catal.* **1987**, *35*, 1.
(11) Iwasawa, Y.; Asakura, K.; Ishii, H.; Kuroda, H. *Z. Phys. Chem. (Munich)* **1985**, *144*, 105.
(12) Bhasin, M. M.; Bartley, W. J.; Ellgen, P. C.; Wilson, T. P. *J. Catal.* **1978**, *54*, 120.
(13) Evans, D.; Osborn, J. A.; Wilkinson, G. J. *J. Chem. Soc. A* **1968**, 3133.
(14) Noack, K.; Calderazzo, F. *J. Organomet. Chem.* **1967**, *10*, 101.
(15) Calderazzo, F. *Angew. Chem., Int. Ed. Engl.* **1977**, *16*, 299.
(16) Collman, J. P.; Rothroch, R. K.; Finke, R. G.; Moore, E. J.; Rose-Munch, F. *Inorg. Chem.* **1982**, *21*, 146.
(17) Casey, C. P.; Cyr, C. R.; Anderson, R. L.; Marten, D. F. *J. Am. Chem. Soc.* **1975**, *97*, 3053.
(18) Morrison, E. D.; Steinmetz, G. R.; Geoffroy, G. L.; Fultz, W. C.; Rheingold, A. R. *J. Am. Chem. Soc.* **1984**, *106*, 4783.
(19) Isobe, K.; Vanzequez de Miguel, A.; Bailey, R. M.; Okeya, S.; Maitlis, P. M. *J. Chem. Soc., Dalton Trans.* **1983**, 1441.
(20) Saez, I. M.; Meanwell, N. J.; Nutton, A.; Isobe, K.; Vanzequez de Miguel, A.; Bruce, D. W.; Okeya, S.; Andrews, D. G.; Ashton, P. R.; Johnstone, I. R.; Maitlis, P. M. *J. Chem. Soc., Dalton Trans.* **1986**, 1565.
(21) Oyanagi, H.; Matsushita, T.; Ito, M.; Kuroda, H. *Natl. Lab. High Energy Phys., KEK (Jpn)* **1984**, *83*-30.
(22) Teo, B. K. *Basic Principles and Data Analysis, Inorganic Chemistry Concepts 9*; Springer-Verlag: Berlin, 1986.
(23) Kosugi, N.; Kuroda, H. EXAFS analysis Program, *EXAFS 2*; Research Center for Spectrochemistry: University of Tokyo.
(24) Teo, B. K.; Lee, P. A. *J. Am. Chem. Soc.* **1979**, *101*, 2815.
(25) Teo, B. K. *J. Am. Chem. Soc.* **1981**, *103*, 3990.

Table II. Temperature-Programmed Decomposition Analysis for the SiO_2-Attached $[Rh(C_5Me_5)(CH_3)]_2(\mu\text{-}CH_2)_2$

	evolved gases per Rh dimer unit		
temp[a]/K	CH_4	C_2H_6	C_2H_4
283–313	0.97	0.0	0.0
313–343	0.03	0.0	0.0
343–373	0.0	0.0	0.0
373–403	0.0	0.0	0.0
403–433	0.05	0.01	0.01

[a] Heating rate: 4 K min^{-1}.

amplitude function. S_j is unity when the empirically derived amplitude function is used. N_j, σ_j, and r_j are the coordination number, the Debye–Waller factor, and interatomic distance, respectively. The fitting parameters are N_j, r_j, ΔE_j (difference between the origin of the photoelectron wave vector and that conventionally determined), and σ_j.

The FT-IR spectra were measured on a JEOL JIR 100 spectrometer. A self-supported SiO_2 disk was placed in an in situ IR cell connected to a closed circulating system. The SiO_2 disk was pretreated at 673 K for 1 h in the cell, and a pentane solution of $[Rh(C_5Me_5)(CH_3)]_2(\mu\text{-}CH_2)_2$ or deuterated dimer complexes was added dropwise onto the SiO_2 disk in a flow of a high-purity Ar.

The gas-phase analysis during the attachment of the complexes and the subsequent thermal decomposition process was carried out in a closed circulating system by a gas chromatograph with 5A molecular sieves and VZ-10 columns.

The catalytic hydroformylation reaction was conducted in a closed circulating system (dead volume, 180 cm^3) under the conditions of $CO:H_2:C_2H_4 = 1:1:1$ (total pressure, 40.0 kPa) at 413 K. The products were analyzed by gas chromatography with use of VZ-10 and DOS columns. For comparison, conventional Rh/SiO_2 catalysts were prepared by impregnation of SiO_2 with aqueous solutions of $RhCl_3$. The samples were dried at 383 K for 3 h. They were then calcined at 773 K for 1 h and were reduced with H_2 at 773 K for 1 h.

Results

Thermal Decomposition Analysis of the Rh Dimer Attached on SiO_2. Table II shows the amount of products evolved after the thermal decomposition of the incipient Rh dimers on SiO_2. Nearly one CH_4 was evolved before 373 K, indicating that a CH_3 ligand of $[Rh(C_5Me_5)(CH_3)]_2(\mu\text{-}CH_2)_2$ was lost by the reaction with the SiO_2 surface at 293–343 K. The formation of ethene and ethane was negligible. No significant formation of C_2H_4 and C_2H_6 was observed in the temperature range 373–433 K. The carbon amount in the products evolved by the thermal decomposition until 773 K and by the subsequent oxidation with O_2 suggested that about 30% of the C_5Me_5 ligands was lost by the attaching reaction with the SiO_2 surface at 293 K. The liquid chromatographic analysis also showed that 25% of the C_5Me_5 was released upon the attachment at 293 K.

IR Studies of the Rh Dimer Complexes and the Attached Species A. Figure 1a shows the IR spectrum of $[Rh(C_5Me_5)(CH_3)]_2(\mu\text{-}CH_2)_2$ in a KBr disk. Several peaks arising from CH_3, $\mu\text{-}CH_2$, and CH_3 of C_5Me_5 were observed in the ν(C–H) and δ(C–H) regions. Since the assignment of C–H frequencies had not been made in the literature, we assigned the observed C–H frequencies using the deuterated Rh dimer complexes. Figure 1b,c exhibits IR spectra of $[Rh(C_5Me_5\text{-}d)(CH_3)]_2(\mu\text{-}CH_2)_2$ and $[Rh(C_5Me_5\text{-}d)(CD_3)]_2(\mu\text{-}CH_2)_2$ in KBr disks, respectively. From the comparison among these spectra in Figure 1a–c, the bands at 2931 and 2864 cm^{-1} are assigned to $\mu\text{-}CH_2$, while the bands at 2877 and 2790 cm^{-1} are assigned to CH_3 ligands, as shown in Table III. The C–H frequencies of $\mu\text{-}CH_2$ and CH_3 in $[Rh(C_5Me_5)(CH_3)]_2(\mu\text{-}CH_2)_2$ are lower than those found in the literature.[26-28]

Since the ν(C–H) region in $[Rh(C_5Me_5)(CH_3)]_2(\mu\text{-}CH_2)_2$ was complex, we studied $[Rh(C_5Me_5\text{-}d)(CH_3)]_2(\mu\text{-}CH_2)_2/SiO_2$ to separate the ν(C–H) peak of C_5Me_5 from those of CH_3 and

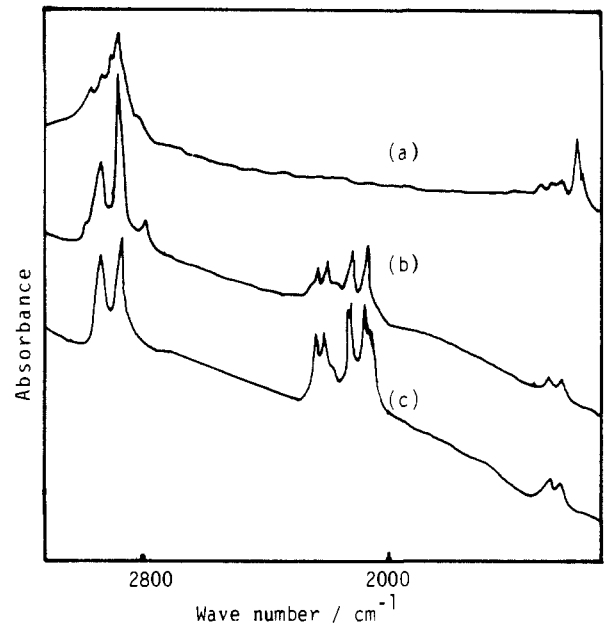

Figure 1. IR spectra of the Rh dimer and the deuterated complexes: (a) $[Rh(C_5Me_5)(CH_3)]_2(\mu\text{-}CH_2)_2$ in KBr, (b) $[Rh(d\text{-}C_5Me_5)(CH_3)]_2(\mu\text{-}CH_2)_2$ in KBr, (c) $[Rh(d\text{-}C_5Me_5)(CD_3)]_2(\mu\text{-}CH_2)_2$ in KBr.

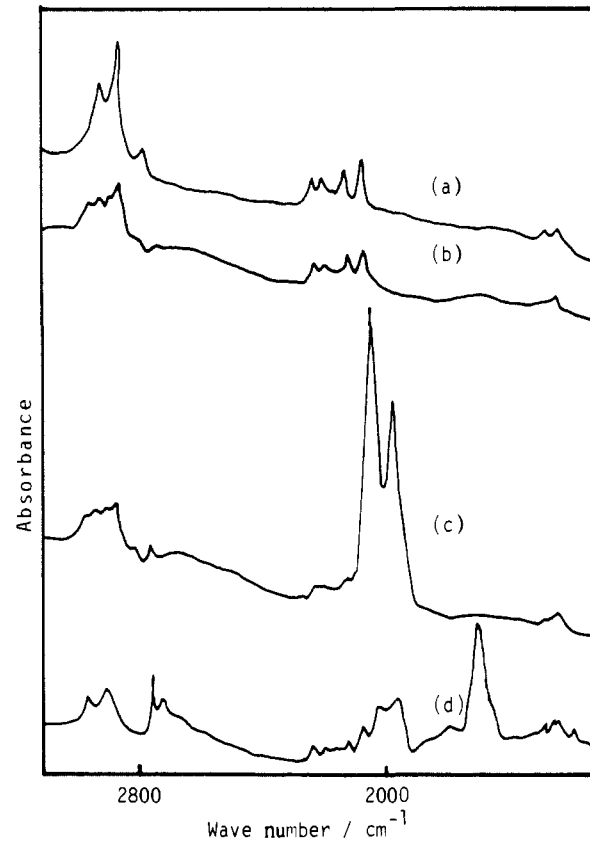

Figure 2. IR spectra of the SiO_2-attached $[Rh(d\text{-}C_5Me_5)(CH_3)]_2(\mu\text{-}CH_2)_2$: (a) treated at 313 K, (b) treated at 373 K, (c) exposed to 40 kPa of CO at 313 K, (d) evacuated at 423 K.

$\mu\text{-}CH_2$. Figure 2a shows the three distinct peaks assigned to $\mu\text{-}CH_2$, $\mu\text{-}CH_2 + CH_3$, and CH_3 ligands, respectively. When the surface Rh dimers were heated to 373 K under vacuum, the intensity of the 2879-cm^{-1} peaks markedly decreased and the 2790-cm^{-1} peak almost disappeared, as shown in Figure 2b. The peak at 2935 cm^{-1} also decreased by half in intensity. On the other hand, new peaks appeared at 2964 and 2912 cm^{-1} in Figure 2b. The corresponding peaks also appeared at 2964 and 2908 cm^{-1} when $[Rh(C_5Me_5\text{-}d)(CD_3)]_2(\mu\text{-}CH_2)_2$ was used instead of [Rh-

(26) Oxton, I. A.; Powell, D. B.; Sheppard, N.; Burgess, K.; Johnson, B. F. G.; Lewis, J. *J. Chem. Soc., Chem. Commun.* **1982**, 719.
(27) Herrmann, W. A.; Riedel, D.; Ziegler, M. L.; Weidenhammer, K.; Guggolz, E.; Balbach, B. *J. Am. Chem. Soc.* **1981**, *103*, 63.
(28) George, P. M.; Avery, N. R.; Weinberg, W. H.; Tebbe, F. N. *J. Am. Chem. Soc.* **1983**, *105*, 1393.

Table III. C–H (C–D) Stretching Frequencies for CH_3 and μ-CH_2 Ligands

sample	ν/cm^{-1} (C–H (C–D))	ref
$[Rh(C_5Me_5)(CH_3)]_2(\mu\text{-}CH_2)_2$	2962 (C_5Me_5), 2935 (μ-CH_2), 2902 (CH_3), 2873 (CH_3 + μ-CH_2), 2790 (CH_3)	this work
$[Rh(C_5Me_5\text{-}d)(CH_3)]_2(\mu\text{-}CH_2)_2$	2935 (μ-CH_2), 2877 (CH_3 + μ-CH_2), 2790 (CH_3)	this work
$[Rh(C_5Me_5\text{-}d)(CD_3)]_2(\mu\text{-}CH_2)_2$	2931 (μ-CH_2), 2864 (μ-CH_2)	this work
C_5Me_5-*d* ligand	2227, 2190, 2115, 2063	this work
$(\mu\text{-}H)_2Os_3(CO)_{10}(\mu\text{-}CH_2)$	2984, 2935	26
$Os_3(CO(_{10}(\mu\text{-}CO)(\mu\text{-}CH_2)$	2990, 2949	26
$(\mu\text{-}CH_2)[(C_5H_5)Rh(CO)]_2$	2963, 2903	27
$(\mu\text{-}CO)_2[Rh_2(C_5H_5)_2(CH_3)Cl]$	2911	27
$(\mu\text{-}CH_2)[(C_5H_5)Co(CO)]_2$	2981, 2918	28

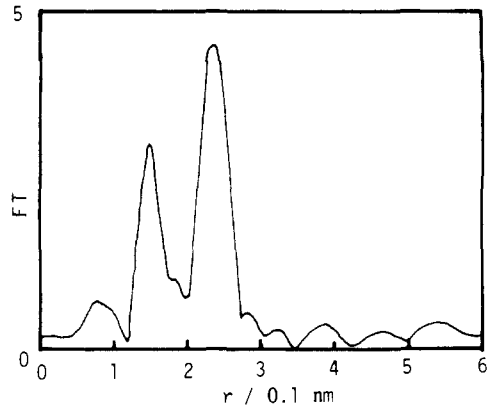

Figure 3. Fourier transform of k^3-weighted EXAFS for $[Rh(C_5Me_5)(CH_3)]_2(\mu\text{-}CH_2)_2$.

$(C_5Me_5\text{-}d)(CH_3)]_2(\mu\text{-}CH_2)_2$, suggesting that these new peaks must have arisen from μ-CH_2. Since the intensities of the peaks for μ-CH_2 and CH_3 decreased to half of their original intensities, one μ-CH_2 and one CH_3 seem to react to form a new ligand like CH_2CH_3, while one μ-CH_2 remained in species A as shown in Figure 5. The peak intensity for CD_3 groups of C_5Me_5-*d* also decreased to the ca. 65% level of that for the incipient surface Rh dimers by heating to 373 K as shown in Figure 2a, suggesting the release of a part of the C_5Me_5-*d* ligand.

EXAFS Studies of the Rh Dimer Complex and the Attached Species A. Figure 3 shows the Fourier transform of k^3-weighted EXAFS data of $[Rh(C_5Me_5)(CH_3)]_2(\mu\text{-}CH_2)_2$ over k = 30–150 nm^{-1}. A main peak in the Fourier transform might be due to Rh–Rh interaction. We carried out curve-fitting analysis on the second Fourier-transformed peak using the Fourier filtering method. The curve-fitting analysis over several different k regions revealed that a Rh–Rh distance was 0.259 ± 0.002 nm. The value, 0.259 nm, is similar to the X-ray crystallographic distances of *cis*-$[Rh(C_5Me_5)(CH_3)]_2(\mu\text{-}CH_2)_2$ (0.262 nm)[19] and *trans*-$[Rh(C_5Me_5)(CH_3)]_2(\mu\text{-}CH_2)_2$ (0.259 nm),[19] though the X-ray analysis of the trans compound has not completely been made. We also carried out the curve-fitting analysis of the first shell in Figure 3. As we did not find a good model compound for the first shell (Rh–C), we used theoretical parameters for the analysis. Although the first coordination shell is composed of three different bondings, three-shell fitting did not give realistic values because of a correlation problem among the fitting parameters. Hence, we carried out one-shell fitting for the first coordination shell of the Rh dimer. The distance obtained from one-shell analysis was 0.205 ± 0.003 nm. This value is in good agreement with 0.203 nm of Rh–C(CH_2) in the Rh dimer complex.[19] This fitting result may be rationalized by the explanation that one-shell fitting of EXAFS data would represent the structural parameters of the most sharply changing part of the distribution curve or those of the coordination shell with a low static disorder.[29] The contribution of the Rh–C(C_5Me_5) to EXAFS oscillation might be small because of large static disorder (0.007 nm). The Rh–C(CH_2) has a larger coordination number than Rh–C(CH_3). Consequently, one-shell-fitting analysis mainly reflects the Rh–C(μ-CH_2) distance.

(29) Eisenberger, P.; Brown, G. S. *Solid State Commun.* **1979**, *29*, 481.

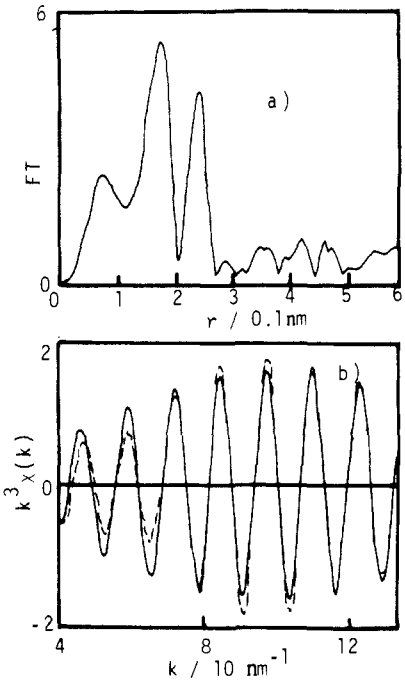

Figure 4. (a) Fourier transform of k^3-weighted EXAFS for species A and (b) the fitting curve for the second coordination shell: —, observed; ---, calculated.

Table IV. Curve-Fitting Results of the EXAFS Data for the Rh-Dimer Complex and the SiO_2-Attached Rh-Dimer Species

sample		CN	r/nm	σ/nm
$[Rh(C_5Me_5)(CH_3)]_2(\mu\text{-}CH_2)_2$	Rh–C	2.0 ± 0.3	0.205 ± 0.003	0.008 ± 0.002
	Rh–Rh	1.0 ± 0.2	0.259 ± 0.002	0.004 ± 0.002
species A	Rh–C	0.8 ± 0.5	0.204 ± 0.003	0.007 ± 0.004
	Rh–O	1.4 ± 0.3	0.220 ± 0.003	0.005 ± 0.002
	Rh–Rh	1.0 ± 0.3	0.262 ± 0.003	0.007 ± 0.002
species B	Rh–C	0.7 ± 0.3	0.203 ± 0.003	0.007 ± 0.004
	Rh–C	0.7 ± 0.2	0.188 ± 0.003	0.006 ± 0.002
	Rh–O	1.4 ± 0.2	0.220 ± 0.003	0.005 ± 0.002
	Rh---O	0.9 ± 0.2	0.299 ± 0.002	0.006 ± 0.003
species C	Rh–C	0.7 ± 0.4	0.205 ± 0.003	0.006 ± 0.003
	Rh–O	1.3 ± 0.3	0.219 ± 0.003	0.005 ± 0.002
	Rh–Rh	0.9 ± 0.3	0.270 ± 0.003	0.008 ± 0.003
species D	Rh–C	0.8 ± 0.2	0.187 ± 0.003	0.006 ± 0.003
	Rh–O	1.4 ± 0.2	0.220 ± 0.003	0.005 ± 0.003
	Rh---O	0.9 ± 0.2	0.299 ± 0.002	0.006 ± 0.003

Figure 4a shows the Fourier transform of the k^3-weighted EXAFS oscillation for the attached Rh dimer A. The second peak at 0.25 nm may be straightforwardly assigned to Rh–Rh bonding. The curve-fitting result for the second peak based on Rh–Rh interaction was given in Figure 4b. A little difference between the fitting curve and the observed one may arise from the limit of transferability in the phase shift and amplitude functions of Rh metal due to the different electronic states. The Rh–Rh distance and the coordination number were determined to be 0.262 ± 0.003 nm and 1.0 ± 0.2 as shown in Table IV. The Debye–Waller factor increased to 0.007 from 0.004 nm for the unsup-

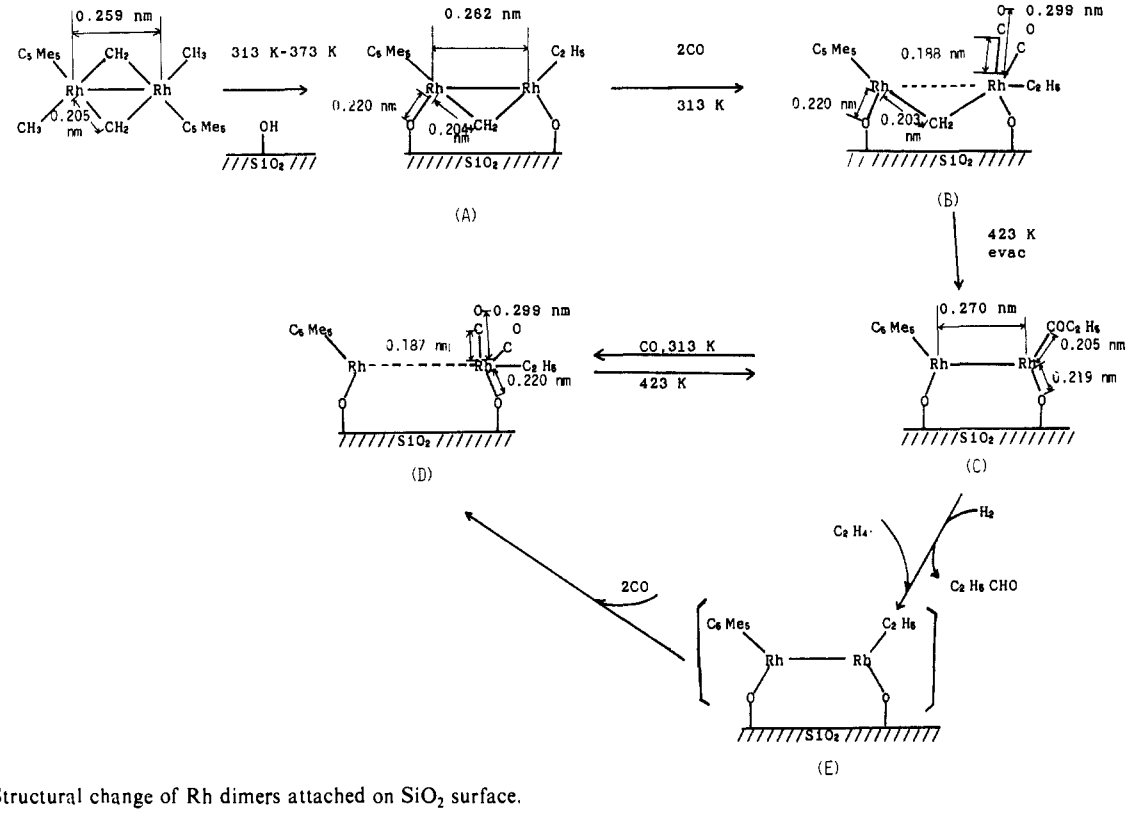

Figure 5. Structural change of Rh dimers attached on SiO_2 surface.

Table V. Catalytic Hydroformylation Reaction at 413 K[a]

catalyst	TOF/10^{-4} min^{-1} total	ethane	propanal	selectivity/% (propanal/total)
impreg catal	10.9	9.9	0.96	8.8
Rh dimer	36.9	4.1	32.8	88.9

[a] C_2H_4:CO:H_2 = 1:1:1 (total pressure, 40.0 kPa).

ported complex $[Rh(C_5Me_5)(CH_3)]_2(\mu\text{-}CH_2)_2$. The fact that the coordination number was unity indicated that the Rh species was attached as a dimer form.

In contrast to the release of some ligands upon attachment, the first peak of $[Rh(CH_3)(C_5Me_5)]_2(\mu\text{-}CH_2)_2$ increased. It can be explained by the formation of a Rh–O bond by the reaction of the Rh dimer with the surface OH groups at 313–373 K. Four-shell fitting (Rh–C(alkyl), Rh–C(μ-CH_2), Rh–C(C_5Me_5) and Rh–O(surface)) did not give reasonable fitting results, owing to the correlation problem as already mentioned. Therefore, we carried out two-shell fitting assuming Rh–C and Rh–O, giving the bond distances at 0.204 ± 0.003 and 0.220 ± 0.003 nm, respectively. The S_j values for Rh–C and Rh–O were derived from the EXAFS data of $[Rh(C_5Me_5)(CH_3)]_2(\mu\text{-}CH_2)_2$ and Rh_2O_3. Although oxygen and carbon atoms cannot be discriminated from each other by comparison with the EXAFS oscillations, the bond at 0.204 nm is most likely to be attributed to Rh–C(μ-CH_2), while the new bond at 0.220 nm can be due to Rh–O(surface) as shown in Figure 5. This distance agrees well with our previous work on inorganic oxide attached noble-metal atoms.[30-34]

Hydroformylation of Ethene on the SiO_2-Attached Rh Dimer Catalyst. The Rh dimer catalyst was found to have a catalytic activity for ethene hydroformylation. The typical results are given in Table V, which shows the turnover frequency and selectivities for ethene hydroformylation on the Rh dimer catalyst. The 30% dispersed impregnated Rh/SiO_2 showed the highest activity for propanal formation among a series of impregnation catalysts, and its result is given in Table V. The attached Rh dimer catalyst was more active and selective for hydroformylation compared with the impregnation catalyst, as shown in Table V.

The catalyst was stable under the reaction conditions at temperatures below 453 K, indicating stationary catalytic activity and selectivity. However, at temperatures higher than 473 K and higher pressures (such as 2 MPa), the dimer structure was suggested to gradually change to small Rh clusters when the Rh–Rh distance was found at 0.264 nm with the coordination number of 5.5 in EXAFS analysis. In order to understand the reason that the dimer structure is active and selective and to explore the role of dimer structures or metal–metal bonds in catalysis, we examined the behaviors of both adsorbed Rh dimer species and Rh sites by in situ IR and EXAFS techniques.

Behavior of Adsorbed Species on the Rh Dimer Catalyst in the Course of Hydroformylation. Figure 2c shows the IR spectrum of species B, which was obtained by exposure of sample A to 40 kPa of CO at room temperature. Two peaks appeared at 2032 and 1969 cm^{-1}, owing to CO stretching vibrations. This feature is contrasted to the unsupported Rh dimer, which did not adsorb CO. In order to characterize the two CO stretching modes, we measured the spectra of ^{13}CO and a mixture of ^{13}CO and ^{12}CO in Figure 6. Adsorbed ^{13}CO exhibited two peaks at 1986 and 1922 cm^{-1} in Figure 6b. If CO adsorbs on two different sites, four peaks should appear independently by the adsorption of a mixture of ^{12}CO and ^{13}CO. On the other hand, if CO is adsorbed as twin type, there are the possibilities of ^{12}CO–^{12}CO, ^{12}CO–^{13}CO, and ^{13}CO–^{13}CO pairs giving six peaks. We admitted an equal mixture of ^{12}CO and ^{13}CO onto the ^{12}CO-preadsorbed Rh dimer for 10 min. At this stage, the replacement of ^{12}CO by ^{13}CO is incomplete and the population for the pair is in the order ^{12}CO–^{12}CO > ^{12}CO–^{13}CO ≫ ^{13}CO–^{13}CO. We could obtain the peaks due to the ^{12}CO–^{13}CO pair by cancellation of the contribution of the ^{12}CO–^{12}CO pair. Figure 6c is the spectrum thus observed, which shows two new peaks at 2019 and 1943 cm^{-1}. The appearance of six peaks indicates that adsorbed CO is of a twin type. A volumetric measurement showed the amount of adsorbed CO to be nearly two per Rh dimer. The unsupported Rh dimer

(30) Asakura, K.; Yamada, M.; Iwasawa, Y.; Kuroda, H. *Chem. Lett.* **1985**, 511.
(31) Asakura, K.; Iwasawa, Y.; Yamada, M. *J. Chem. Soc., Faraday Trans. 1* **1988**, *84*, 2457.
(32) Asakura, K.; Iwasawa, Y.; Kuroda, H. *Bull. Chem. Soc. Jpn.* **1986**, *59*, 647.
(33) Asakura, K.; Iwasawa, Y.; Kuroda, H. *J. Chem. Soc.* **1988**, *84*, 1329.
(34) Duivenvooden, F. B. M.; Koningsberger, D. C.; Uh, Y. S.; Gates, B. C. *J. Am. Chem. Soc.* **1986**, *108*, 6254.

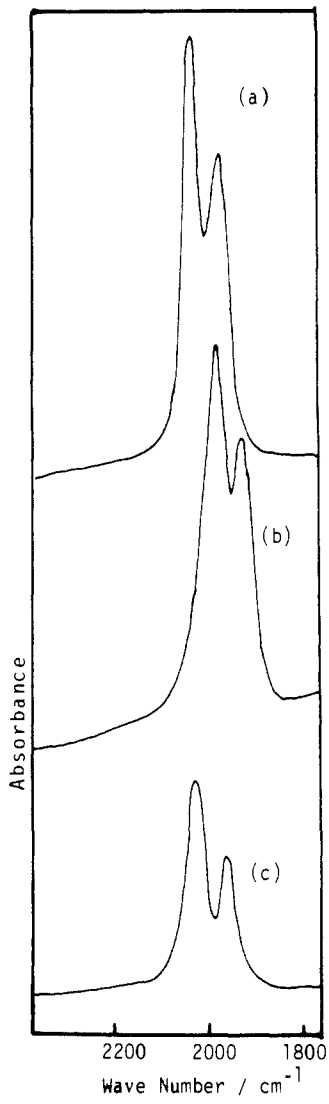

Figure 6. IR spectra of CO adsorbed on the Rh species B: (a) Rh(^{12}CO)(^{12}CO), (b) Rh(^{13}CO)(^{13}CO), (c) Rh(^{12}CO)(^{13}CO).

complex did not adsorb any CO, which implies that a large C_5Me_5 ligand blocks CO adsorption on the Rh atom. Thus, a Rh atom with an alkyl group is suggested to adsorb CO in a twin form as shown in Figure 5.

When sample B was heated at 423 K under vacuum, the twin peak almost disappeared and new peaks appeared at 1710 and 1394 cm^{-1} as shown in Figure 2d. In this stage, the peaks for carbenes almost diminished, and the peaks at 2962 and 2910 cm^{-1} assignable to alkyl groups were observed. Figure 7b shows the variation of the peak intensities at 1969 and 1710 cm^{-1} with evacuation time at 423 K. The initial rates of the increase in the peak intensity at 1710 cm^{-1} and the decrease in the peak intensity at 1969 cm^{-1} were almost the same (8.3×10^{-2} min^{-1}). About one CO molecule was evolved during the evacuation, leaving one CO on a Rh dimer. Judging from the frequencies and the composition of Rh dimer C, the peak at 1710 cm^{-1} could be attributed to ν(CO) of the acyl (propanoyl) group on the Rh atom, while the peak at 1394 cm^{-1} is assigned to δ(CH) of the acyl group. In fact, ν(CO) for acyl groups in $(AsPh_4)[RhI(COEt)(PPh_3)(mnt)]$, $[RhCl_2(COEt)(PPh_3)_2]_2$, and $Rh(COMe)(CO)_2L_2$ have been reported in the range 1679–1710 cm^{-1}.[35-37] The peak at 2964 cm^{-1} of the alkyl group for the twin CO–Rh species decreased by heating at 423 K, while the peak at 2910 cm^{-1} increased. These data on the spectrum change suggest that one of the twin CO ligands reacted with a C_2H_5 to form a C_2H_5CO group (CO insertion) as shown in structure C Figure 5. In fact, species C reacted with H_2 to form propanal.

Figure 8a is the same spectrum as Figure 2d for species C. When species C was exposed to CO at 290–313 K, the twin CO peaks were regenerated with the concomitant disappearance of the acyl peaks at 1710 and 1394 cm^{-1} as shown in Figure 8b. When sample C with ^{12}CO was exposed to ^{13}CO, a spectrum similar to Figure 6c was observed, indicating the presence of Rh(^{12}CO)(^{13}CO) species. Thus, one CO comes from the gas phase, and the other arises from decarbonylation of the acyl group.

When the sample having the twin CO (Figure 8b) was heated at 423 K under vacuum, the peaks corresponding to acyl ligands reappeared, while the twin carbonyl peaks almost disappeared, as shown in Figure 8c. At the same time, the peak at 2964 cm^{-1} decreased and the peak at 2910 cm^{-1} increased. These phenomena were completely reversible. Note that the feature is entirely different from mononuclear metal chemistry as discussed hereinafter.

In Situ EXAFS Observation of the Rh Sites during Adsorption and Reaction. As shown in Figure 9, the Fourier transforms of species B–D in Figure 5 consist of two main peaks. Three-shell-fitting analysis (Rh–C(μ-CH_2), Rh–C(CO), and Rh–O(surface)) was performed for the first shell of the Fourier transform for species B by use of theoretical parameters. The Rh–C bondings for C_2H_5 and C_5Me_5 groups were neglected as mentioned for the analysis of the unsupported Rh dimer $[Rh(C_5Me_5)(CH_3)]_2(\mu\text{-}CH_2)_2$. From the EXAFS analysis, the distances for Rh–O(surface), Rh–C(μ-CH_2), and Rh–C(CO) were determined to be 0.220 ± 0.002, 0.203 ± 0.003, and 0.188 ± 0.003 nm, respectively. The bond distances of Rh–O and Rh–C were similar to those for species A, and the bond distance of Rh–C(CO) was also similar to those of Rh–CO distances reported in the literature.[38-40] IR spectra for species C showed loss of the μ-CH_2 ligand and formation of the acyl group. Thus, we carried out the two-shell fitting of Rh–C(COC_2H_5) + Rh–O(surface), where Rh–C_5Me_5 can be neglected. The Rh–O and Rh–C bonds were observed at 0.219 ± 0.003 and 0.205 ± 0.005 nm, respectively, as shown in Table IV. The Rh–C distance is similar to that of Rh–C(COMe) in $[Me_3PhN][Rh_2I_2(COMe)_2(CO)_2]$.[41] Similarly, for species D in Figure 5, two-shell-fitting analysis (Rh–O(surface) and Rh–C(CO)) was performed and the result is given in Table IV.

At the next step, we carried out the analysis for the second shell of Fourier transforms (in Figure 9). The Fourier transform for species B is similar to that for species A as shown in Figure 4 and Figure 9a. However, the EXAFS oscillation for species B was different from that for species A. Figure 10 showed the k-weighted EXAFS oscillations for species A–D. The EXAFS oscillation for species B almost diminished in the k region higher than 90 nm^{-1}, suggesting the absence of a heavy scatterer such as Rh atom around a Rh absorber. We carried out a curve-fitting analysis for the second peak of the Fourier transform for species B, assuming it is due to Rh---O(carbonyl) and/or Rh–Rh bonding. A good fitting result was obtained only based on Rh---O(carbonyl) rather than Rh–Rh as shown in Figure 11, where the Rh---O distance was determined to be 0.299 ± 0.002 nm.

Figure 9c showed the Fourier transform for species C, which has an acyl ligand. The Fourier transform is not definitely different from the transforms of Figure 9b, but the second peak can be ascribed to Rh–Rh because the EXAFS oscillation appeared again at the high-k region as shown in Figure 10c. The best fit

(35) Cheng, C. H.; Spivack, B. D.; Eisenberg, R. *J. Am. Chem. Soc.* **1977**, *99*, 3003.
(36) Baurd, M. C.; Maguc, J. T.; Osborn, J. A.; Wilkinson, G. *J. Chem. Soc., A* **1967**, 1347.
(37) Hegedus, L. S.; Kendall, P. M.; Lo, S. M.; Sheats, J. R. *J. Am. Chem. Soc.* **1975**, *97*, 5448.
(38) Isobe, K.; Okeya, S.; Meanwell, N. J.; Smith, A. J.; Adams, H.; Maitlis, P. M. *J. Chem. Soc., Dalton Trans.* **1984**, 1215.
(39) Corey, E. R.; Dahl, L. F. *J. Am. Chem. Soc.* **1963**, *85*, 1202.
(40) Van't Blik, H. F. J.; van Zon, J. B. A. D.; Huizinga, T.; Vis, J. C.; Koningsberge, D. C.; Prins, R. *J. Am. Chem. Soc. 107*, 3139.
(41) Adamson, G. W.; Daly, J. J.; Foster, D. *J. Organomet. Chem.* **1974**, *71*, C17.

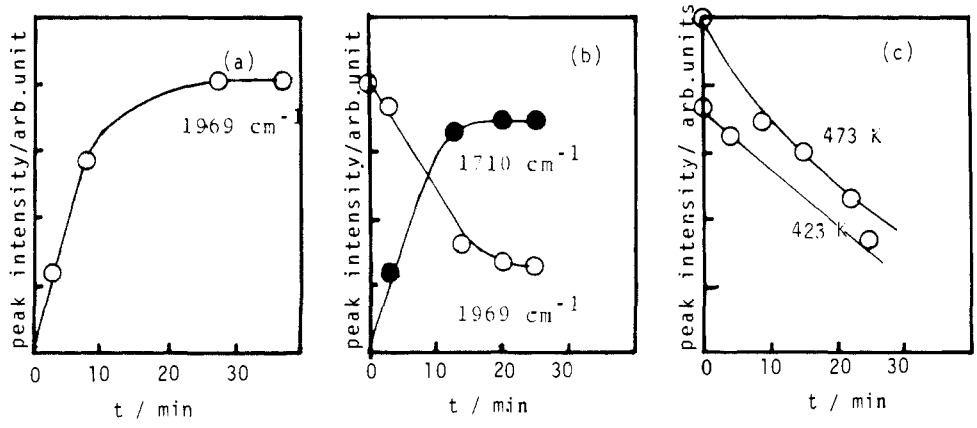

Figure 7. Variations of the IR peaks with reaction time: (a) CO adsorption, (b) CO insertion, (c) reaction of acyl group with H_2.

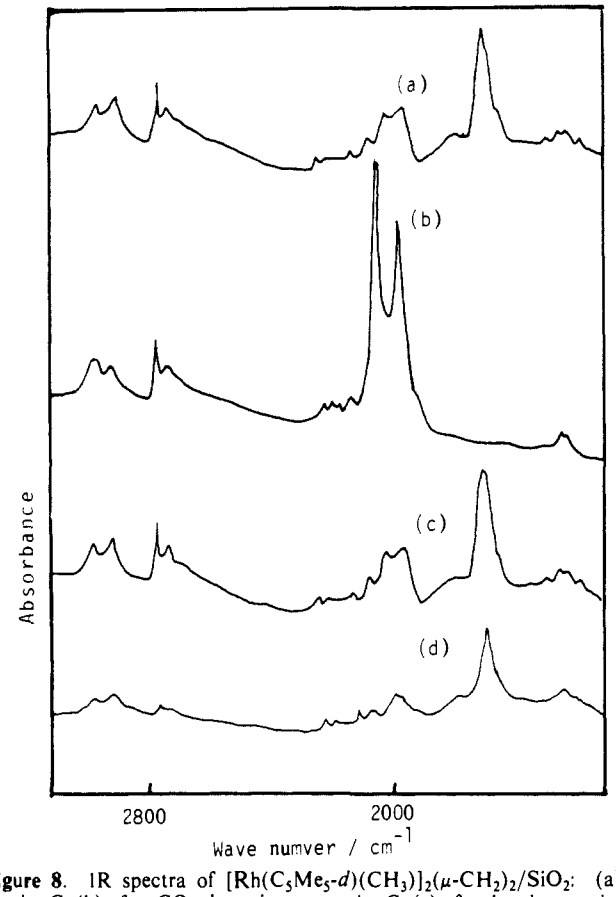

Figure 8. IR spectra of $[Rh(C_5Me_5\text{-}d)(CH_3)]_2(\mu\text{-}CH_2)_2/SiO_2$: (a) species C, (b) after CO adsorption on species C, (c) after heating species D at 423 K under vacuum, (d) after reaction of species C with H_2 for 10 min at 425 K.

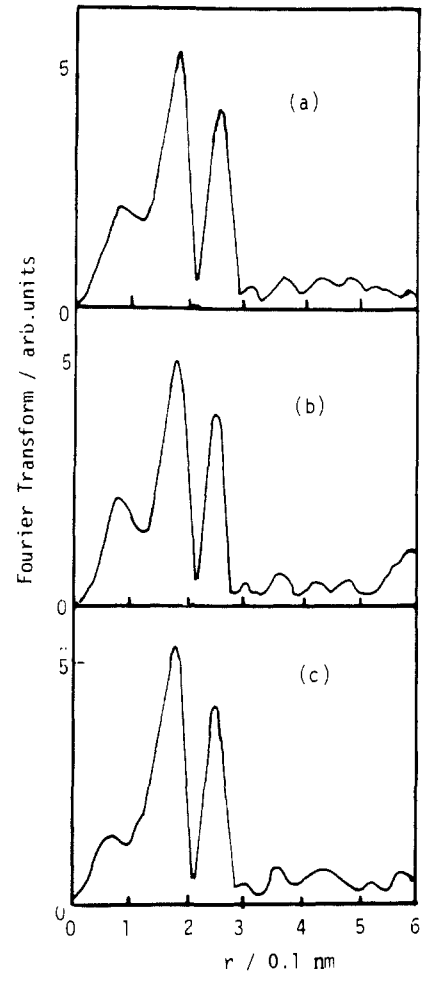

Figure 9. Fourier transforms of Rh K-edge EXAFS: (a) species B, (b) species C, and (c) species D.

result was obtained on the basis of Rh–Rh bonding at 0.270 ± 0.002 nm. When sample C was exposed to 65 kPa of CO, the EXAFS oscillation at the high-k range diminished again as shown in Figure 10d, indicating the cleavage of the Rh–Rh bond in species D as shown in Table IV. We also measured the EXAFS spectrum on sample D at 77 K in order to reduce thermal disorder. Again, no Rh–Rh bond was observed at the low temperature.

Discussion

The structure of the attached Rh dimer A and its structural change are illustrated in Figure 5.

When the Rh dimer complex is attached onto SiO_2 at 313 K, one methane per Rh dimer was evolved as shown in Table II. Twenty-five percent of the C_5Me_5 ligands was released by the attachment at 293 K, and about 35% of the remaining C_5Me_5 ligands was lost by the subsequent heating to 373 K under vacuum from IR results. Hence, half of C_5Me_5 ligands in $[Rh(C_5Me_5)(CH_3)]_2(\mu\text{-}CH_2)_2$ was released at 373 K. The intensity of the Si–OH peak at 3740 cm^{-1} decreased by attaching the dimer complex SiO_2. These results demonstrated that the *trans*-$[Rh(C_5Me_5)(CH_3)]_2(\mu\text{-}CH_2)_2$ was chemically bound to the SiO_2 surface by the reaction with surface OH groups, liberating one CH_3 and one C_5Me_5 per Rh dimer. The observation of the new Rh–O bond at 0.220 nm in Table III confirms the chemical attachment. The 2790-cm^{-1} peak for the CH_3 ligand on Rh disappeared at 373 K with the concomitant decrease of the $\mu\text{-}CH_2$ peak at 2935 cm^{-1} to half the level of the original intensity as shown in Figure 2b. At the same time, the new peaks at 2964 and 2912 cm^{-1}, assignable to an ethyl group, developed. In order to examine this peak change in the ν(CH) region, $[Rh(C_5Me_5\text{-}d)(CD_3)]_2(\mu\text{-}CH_2)_2$ was attached to SiO_2, where the only ν(CH) band observed is due to the $\mu\text{-}CH_2$ group. The peaks at 2935 and 2874 cm^{-1} for the $\mu\text{-}CH_2$ groups decreased by half in intensity,

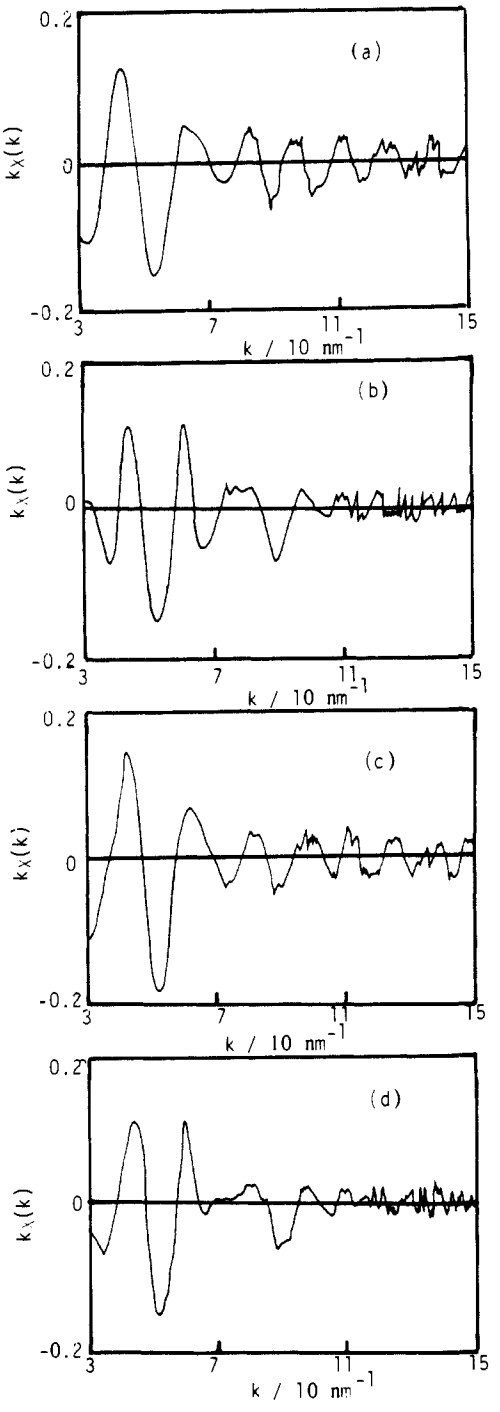

Figure 10. *k*-Weighted EXAFS oscillations: (a) sample A, (b) sample B, (c) sample C, and (d) sample D.

and new peaks at 2964 and 2908 cm^{-1} appeared that are assignable to the μ-CH_2 of the ethyl (CH_2CD_3) ligand on Rh. Thus, the CH_3 ligand reacted with one μ-CH_2 group (carbene insertion) to form an ethyl group as shown in Figure 5 (species A). The curve-fitting analysis of the EXAFS data for species A showed the presence of a Rh–Rh bond at 0.262 nm, and the coordination number was found to be 1, which demonstrates the retention of the dimer structure. The IR data were almost the same for the samples with Rh loadings from 0.7 to 2 wt %, suggesting that the formation of other Rh structures like decomposed monomers on the SiO_2 employed is negligible.

When Rh dimers A were exposed to CO at 313 K, twin carbonyls were formed as shown in Figure 2c and 6. Upon CO adsorption, the Rh–Rh bond was found to be broken as shown in Figures 9 and 10 and in Table IV. Oxidative fragmentation of Rh clusters on Al_2O_3 upon CO adsorption has been reported,[4] but the present observation is different from this phenomenon.

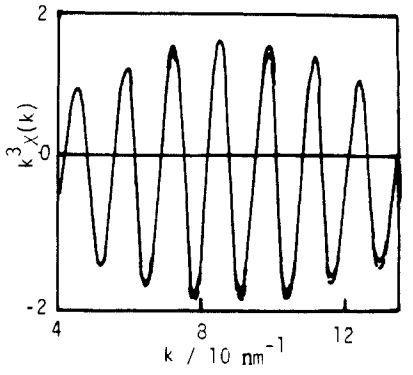

Figure 11. Curve-fitting results for the second peak of the Fourier transform of sample B: —, observed; ---, calculated.

When sample B was heated at 423 K under vacuum, the twin CO bands disappeared and a new peak appeared at 1710 cm^{-1} together with a small peak at 1394 cm^{-1} as shown in Figure 2, indicating the formation of acyl group as shown in Figure 5 species C. The Rh–C(acyl) bond at 0.205 nm is compatible with the Rh–C bond distances (0.201–0.206 nm) reported thus far.[41] Furthermore, the ν(CO) of 1710 cm^{-1} is similar to those (1679–1701 cm^{-1}) observed with Rh complexes.[35-37] The formation of the acyl ligand in species C is also confirmed by the reaction with H_2 at 423 K (step C → step E in Figure 5) as shown in Figure 8d, where propanal was produced, showing a decrease in the peak at 1710 cm^{-1}. The EXAFS oscillation above k = 90 nm^{-1} due to the Rh–Rh bond reappeared in Figure 10c. The EXAFS analysis indicated the existence of a Rh–Rh bond at 0.270 nm with coordination number ~1.

When sample C was exposed to CO, the EXAFS oscillation due to the Rh–Rh bond in Figure 10d disappeared and the twin CO peaks appeared, accompanied by the disappearance of the acyl peak as shown in Figure 8b. The spectral changes between Figure 8a and b and Figure 10c and d were completely reversible. The reversible structural change of Rh sites is illustrated in Figure 5 species C and D.

The chemistry found with the Rh dimers on SiO_2 is unusual and entirely different from the chemistry established on mononuclear metal complexes. In general, CO-insertion reaction on mononuclear metal complexes proceeds favorably at high CO pressures and reverse decarbonylation of acyl takes place under vacuum.[14,15] The CO insertion (ethyl migration) observed with the surface Rh dimers was converse, where CO inserted into the Rh–ethyl bond to form the acyl ligand under vacuum and the acyl group was decarbonylated in the presence of ambient CO. In situ EXAFS study revealed that the Rh–Rh bond of the attached Rh dimers was cleaved by CO adsorption to form twin carbonyls (Figure 5 species D) and in turn it was reformed (0.270 nm) when the acyl group was formed by CO insertion. It is to be noted that species B and D with no Rh–Rh bonding do not act as monomers; in other words, no CO insertion is observed on Rh monomers B and D without Rh–Rh bonding, unlike mononuclear metal-complex catalysts. CO insertion is usually accompanied by the coordination of an additional ligand to occupy the vacant site left after CO insertion (alkyl migration).[14] In the case of the Rh dimers, the vacant site after the CO insertion is occupied by the Rh–Rh bond. Thus, it can be said that the CO-insertion reaction on the attached Rh dimer occurs by the assistance of the Rh–Rh bonding formation. A similar metal-promoted CO insertion[16] has been observed with $Na_2[Fe_2(\mu\text{-}PPh_2)_2(CO)_6]$ with no direct Fe–Fe interaction (Fe---Fe = 0.363 nm,[42] which reacted with RX (R = alkyl) to form $Na[Fe_2(\mu\text{-}PPh_2)_2(CO)_5(COR)]$, accompanied by Fe–Fe bond formation at 0.272 nm.[43] However, this reaction requires an alkyl supply in the form of RX, and neither reversible

(42) Ginsbug, R. E.; Rothrock, R. K.; Finke, R. G.; Collman, J. P.; Dahl, L. F. *J. Am. Chem. Soc.* **1979**, *101*, 6550.
(43) Gindsbug, R. E.; Berg, J. M.; Finke, R. G.; Collman, J. P.; Hodgson, K. O.; Dahl, L. F. *J. Am. Chem. Soc.* **1979**, *101*, 7218.

decomposition of the acyl (COR) nor further reaction with H_2 to form RCHO takes place. The presence of a Rh–O–Si bond would stabilize the Rh dimer structure on the SiO_2 surface and assures the reversible metal-assisted formation and decomposition of acyl group in the SiO_2-attached Rh dimers.

The present work demonstrated that the CO-insertion reaction, which is a key step in ethene hydroformylation, is promoted by metal–metal interaction at the metal surface. Another type of the promotion of CO insertion through the direct bonding of CO molecules with Lewis acids added as cocatalyst (metal–CO- - - Lewis acid) has been proposed.[44,45] However, the metal-assisted CO-insertion mechanism proposed here is essentially different from that the Lewis-acid promoter effects. The metal-assisted mechanism would be the other case to explain the role of metal ensembles in metal catalysis.

The new Rh dimer catalyst was a selective catalyst for ethene hydroformylation as compared with a usual impregnation Rh catalyst as shown in Table V. The activity for the hydrogenation of ethene to form ethane was similar to that of the impregnation catalyst (TOF = 9.9×10^{-4} min^{-1} at 413 K), while the formation of propanal on the Rh dimer catalyst was enhanced by a factor of 30 as compared with the impregnation catalyst. The hydroformylation reaction involves three important elementary reaction steps, CO adsorption, CO insertion, and hydrogenation, as shown in Figure 5. The initial rates of each step could be determined by the changes of IR peaks for CO (1969 cm^{-1}) and acyl (1710 cm^{-1}) groups as shown in Figure 7. The TOF for each step decreased in the order CO adsorption to form twin carbonyls (2×10^{-1} min^{-1} at 313 K) > CO insertion to form acyl group (8.3×10^{-2} min^{-1} at 423 K) > hydrogenation to form propanal (1.0×10^{-2} min^{-1} at 423 K). The steady-state overall reaction rate for propanal formation was much lower than the rates of the three reaction steps. The transformation between species C and species E is reversible, as proved by the observation of IR spectra at various CO pressures. The concentration of intermediate C under catalytic reaction conditions is estimated to be about 3% of the total Rh atoms.

The present combination study of in situ EXAFS and in situ FT-IR techniques revealed the dynamic change of the structure of Rh dimers on the SiO_2 surface during the course of ethene hydroformylation. The chemically designed metal catalysts provide molecular level information on the genesis of essential factors for metal catalysis and, hence, basic implications for developments of new types of catalysts.

Acknowledgment. We thank Prof. M. Nomura and PF staffs for their technical assistance in measuring EXAFS spectroscopy. The EXAFS experiments were carried out under the approval of the EXAFS program committee (Proposal No. 87011).

(44) Richmond, T. G.; Basolo, R.; Shriver, D. F. *Inorg. Chem.* **1982**, *21*, 272.
(45) Ichikawa, M.; Lang, A. J.; Shriver, D. F.; Sachtler, W. M. H. *J. Am. Chem. Soc.* **1985**, *107*, 7216.

Experimental and Modeling Study of Oscillations in the Chlorine Dioxide–Iodine–Malonic Acid Reaction[1]

István Lengyel,[2] Gyula Rábai,[2] and Irving R. Epstein*

Contribution from the Department of Chemistry, Brandeis University, Waltham, Massachusetts 02254-9110. *Received April 11, 1990*

Abstract: At pH 0.5–5.0, a closed system containing an aqueous mixture of chlorine dioxide, iodine, and a species such as malonic acid (MA) or ethyl acetoacetate, which reacts with iodine to produce iodide, shows periodic changes in the light absorbance of I_3^-. This behavior can be modeled by a simple scheme consisting of three component reactions: (1) the reaction between MA and iodine, which serves as a continuous source of I^-; (2) the reaction between $ClO_2^{\bullet}$ and I^-, which acts as a source of ClO_2^-; and (3) the self-inhibited reaction of chlorite and iodide that kinetically regulates the system. The fast component reaction between chlorine dioxide and iodide ion was studied by stopped-flow spectrophotometry. The rate law is $-[ClO_2^{\bullet}]/dt = 6 \times 10^3$ (M^{-2} s^{-1})$[ClO_2^{\bullet}][I^-]$. A two-variable model obtained from the empirical rate laws of the three component reactions gives a good description of the dynamics of the system. The oscillatory behavior results not from autocatalysis but from the self-inhibitory character of the chlorite–iodide reaction.

Introduction

The reaction between iodide ion and chlorite ion exhibits a remarkable variety of kinetic phenomena. These include bistability and oscillatory behavior in a continuous-flow stirred-tank reactor (CSTR),[3] propagating waves in excitable media,[4] stirring and mixing effects on the behavior in a CSTR,[5] critical slowing down,[6] and stochastic behavior.[7] By introducing an additional reactant that can react to regenerate the iodide consumed during each cycle of oscillation, De Kepper et al.[8] constructed the chlorite–iodate–thiosulfate and the chlorite–iodide–malonic acid (MA) systems, which oscillate in a closed (batch) as well as in an open (flow, CSTR) system. Ouyang[9] has carried out a detailed experimental study of the ClO_2^-–I^-–MA reaction. Recently, this reaction has been found to show[10] the symmetry-breaking, reaction-diffusion structures predicted by Turing[11] nearly 40 years ago.

(1) Systematic Design of Chemical Oscillators. 67. Part 66: Simoyi, R. H.; Manyonda, M.; Masere, J.; Mtambo, M.; Ncube, I.; Patel, H.; Epstein, I. R.; Kustin, K. *J. Phys. Chem.*, in press.
(2) Permanent address: Institute of Physical Chemistry, Kossuth Lajos University, H-4010 Debrecen, Hungary.
(3) Dateo, C. E.; Orbán, M.; De Kepper, P.; Epstein, I. R. *J. Am. Chem. Soc.* **1982**, *104*, 504.
(4) Weitz, D. M.; Epstein, I. R. *J. Phys. Chem.* **1984**, *88*, 5300.
(5) (a) Roux, J. C.; De Kepper, P.; Boissonade, J. *Phys. Lett.* **1983**, *97A*, 168. (b) Menzinger, M.; Boukalouch, M.; De Kepper, P.; Boissonade, J.; Roux, J. C.; Saadaoui, H. *J. Phys. Chem.* **1986**, *90*, 313. (c) Luo, Y.; Epstein, I. R. *J. Chem. Phys.* **1986**, *85*, 5733.
(6) Laplante, J. P.; Borckmans, P.; Dewel, G.; Gimenez, M.; Micheau, J. C. *J. Phys. Chem.* **1987**, *91*, 3401.
(7) Nagypál, I.; Epstein, I. R. *J. Chem. Phys.* **1988**, *89*, 6925.
(8) De Kepper, P.; Epstein, I. R.; Kustin, K.; Orbán, M. *J. Phys. Chem.* **1982**, *86*, 170.
(9) Ouyang, Q. Ph.D. Thesis, University of Bordeaux, 1989.
(10) Castets, V.; Dulos, E.; Boissonade, J.; De Kepper, P. *Phys. Rev. Lett.* **1990**, *64*, 2953.

0002-7863/90/1512-9104$02.50/0